

Forecasting Research

Forecasting Research Division
Technical Report No. 207

**A Sensitivity Study of the Single Column UM
to assess which potentially observable quantities
are the most critical to the forecast of fog.**

by

W P Hopwood and P A Clark

January 1997

**Meteorological Office
London Road
Bracknell
Berkshire
RG12 2SZ
United Kingdom**

**Forecasting Research
Technical Report No. 207**

**A Sensitivity Study of the Single Column
UM to assess which potentially observable
quantities are the most critical to the forecast
of fog.**

by

W.P.Hopwood & P.A.Clark.

January 1997

**Forecasting Research
Meteorological Office
London Road
Bracknell
Berkshire
RG12 2SZ
United Kingdom**

©Crown Copyright 1997

This paper has not been published and should be regarded as an Internal Report from the Meteorological Office. Permission to quote from it should be obtained from the above Meteorological Office division.

Abstract.

A project has been under way to build a Site Specific Forecast Model (SSFM) using the single column version of the UM (USCM) as a basis, with suitable modifications (Clark *et al.*, 1996), driven by output from 3D NWP models. This project as part of its first and second stages prepared contributions to the European Commission sponsored project 4MIDaBLE (4-D Meteorological Information Databases Linked across Europe). The first contribution to the 4MIDaBLE project assessed the suitability of the USCM as a fog forecasting model the results of which were also reported in the end of stage 1 report to the SSFM project (Clark *et al.*, 1996). This report contains the final contribution to the 4MIDaBLE project and summarises a sensitivity study of the modified USCM to assess which potentially observable quantities are the most critical to the forecast of fog. This was achieved by intercomparing model forecasts, whose initial conditions were provided by various combinations of observational data, with observations at two sites.

The most important conclusions from this study are as follows:

1. The most important observations are those of humidity because,
 - a) the model is sensitive to changes in humidity,
 - b) the large scale model does quite well with wind and to some extent temperature.
2. The local impact of observations lasts only a few hours since even in light wind cases advection brings in the large scale air after 6 hours.
3. Forecasts initialised late in the afternoon are much more successful at predicting the onset of fog than from earlier in the day.
4. Observations must also improve the larger scale forecast if benefit is to be gained beyond about 3 hours.

A Sensitivity Study of the Single Column UM to assess which potentially observable quantities are the most critical to the forecast of fog.

1 Introduction.

The assessment of the single column version of the Meteorological Office's Unified Model (USCM) as a site-specific forecast model was carried out as stage 1 of the SSFM project and discussed in the end of stage 1 report (Clark *et al.*, 1996). As was cited in that report the use of the USCM was part of a project to develop a high resolution 1D model embedded within the Mesoscale model to provide more site-specific forecast guidance. A description of the Mesoscale model was provided in Clark *et al.* (1996) it will not be repeated here. However as a result of the deficiencies in the USCM identified in Clark *et al.* (1996) the improvements there discussed, to the method of forcing the single column model and its parametrizations, have been implemented. These improvements will be documented and assessed with respect to the model configuration used to derive the results for Clark *et al.* (1996) in a section describing the current 'state of the art'.

The main part of this report will describe a sensitivity study to assess which observable quantities are most critical to the initial conditions of a forecast to provide accurate prediction of visibility at a specified time in the model's integration. The sensitivity study was carried out using four case studies where observational data was available throughout the forecast period. Two of these case studies were provided by Meteo-France, Lille from their observational campaign at Lesquin airport, near Lille, during the winter of 1991/92. The other two case studies were from the Met. Research Unit (MRU) at Cardington, U.K. during the winter of 1995/96 with observations taken from the BALTHUM tethered balloon experiment. A more elaborate description of the observational sites and the measurements taken is detailed below.

2 Experimental Method: Observational Data Acquisition and Production of Model Initial Analyses.

The method of acquiring observational data and the production of model analyses is described. The periods chosen for this study are: 11/12 December 1995 and 2/3 April 1996 for observational data taken at MRU, Cardington; 27/28 November 1991 and 12/13 December 1991 for observational data at Lesquin airport, Lille.

2.1 Observational Data Acquisition

2.1.1 Cardington, U.K.

The Cardington site is an open area of flat grassland that used to be an airfield. To the south-west, the prevalent wind direction, beyond the airfield (~400m from the balloon tether point) the area is dominated by large arable fields up to a distance of approximately 10km from the balloon tether point. The small town of Bedford is situated 6km to the west and to the east and south-east, at a distance of 5-10km, there is a small ridge in the terrain of about 50m in height. The area-average roughness length for the area surrounding the site is 0.005-0.01m

with a soil thermal conductivity of $0.3\text{Wm}^{-1}\text{K}^{-1}$.

The observations taken at this site (52.6°N , 0.25°W) were made using the Cardington tethered balloon facility. The balloon system has been described in detail by Lapworth and Mason (1998) so only a brief description will be given here.

The balloon is a 665 m^3 , helium-filled kite balloon nominally inflated to give around 300 kgf of static lift. Dynamic forces also provide additional lift that limits the windspeed in which the balloon can be operated. The tether cable is a 6 mm diameter steel rope onto which the turbulence probes can be clamped so that they are free to rotate. The balloon system enables instruments to be lifted to heights of over 1 km.

The 'standard' turbulence probe itself consists of a main rectangular package containing an aneroid pressure transducer, pitch and roll inclinometers, signal conditioning and encoding electronics and a low power 400 MHz radio transmitter. In addition rechargeable batteries provide power allowing nominal operating times of between 8 and 10 hours, although this can be extended via the use of additional external battery packs. External to the housing three Gill propeller anemometers, arranged around a cone with a 60° opening angle, are attached to measure the wind vector relative of the probe. In the centre of the propeller array is a platinum resistance thermometer to provide fast-response temperature measurements. The Gill array is kept pointing into wind by a vane which has a three-axis fluxgate magnetometer mounted about halfway along its length. Also attached to the outside of the package is an aspirated housing containing wet and dry bulb thermistors, except on three probes where the wet bulb thermistor had been replaced by a humicap humidity sensor that provides a direct output of the relative humidity.

The outputs from the sensors are digitized at 20 Hz by a 12 bit A/D converter, encoded and then transmitted by radio to a ground station, which separates the signals from different probes, decodes them and passes them to a MicroVax II computer for subsequent storage and processing. For the data presented here only one in twenty records was saved giving an effective sampling rate of 1 Hz.

It should be noted that under certain weather conditions observations either cannot be made or are seriously degraded with this system. Such conditions are: mean windspeed above 17ms^{-1} (35 knots), high lightning risk quantified as Lightning Risk 1 or 2 under the Lapworth system of assessment (Lapworth, 1994) and in rain which serves to damage the PRT's and decrease the lift available to the balloon.

The observations made for this study were obtained with the turbulence probe system being used in its 'Balthum' configuration. Here one turbulence probe is fixed to the balloon tether approximately 150m below the balloon to minimize cable oscillation induced by variations in the magnitude of the dynamic lift gained by the balloon. The turbulence probe is then continuously profiled between the surface and about 1300m. The ascent/descent rate is kept constant at 30 metres per minute giving a profile completion time of about 45 minutes. When weather conditions permit the 'flying' of the balloon, profiling begins at about 0700 UTC continuing to ~1100 UTC and at ~1300 UTC continuing until ~1530 UTC.

Two observational cases have been chosen: 11/12-xii-1995 and 2/3-iv-1996. Both these cases

are situations with little nocturnal cloud, no fog formation in the April case and mist/fog in the December case. Synoptic data for the two observational cases is provided by an automatic (ESAWS) weather station situated some 6km to the North-East of Cardington (52.13°N, 0.29°W). It must be noted that the site where the synoptic data was taken is 50m above the site of the model forecast.

2.1.2 Lesquin Airport, Lille, France.

The Lesquin airport site is similar to the Cardington site in that it consists of an open area of grassland associated with an airport facility. It is situated to the south-east of the town of Lille in North-East France. An area-average roughness length for the area surrounding the site has been associated as 0.005-0.01m with a soil thermal conductivity of $0.3\text{Wm}^{-1}\text{K}^{-1}$.

The observations taken at this site (50.5°N, 3.0°E) have been documented in Guedalia and Bergot (1994). Briefly these consist of: radiosonde ascents conducted at 15Z and 21Z, which retrieve wind, temperature and relative humidity information; mast data at 80m, 45m, 20m, 10m, 5m and 0.7m of temperature (ventilated platinum resistance thermometer), humidity (capacitive sensor), windspeed (cup anemometer), wind direction (wind vane) and visibility (visiometer) were provided with a data acquisition frequency of 0.003Hz.

Two observational cases have been chosen: 27/28-xi-1991 and 12/13-xii-1991. Here the November case has fog formation while the December case produces no fog.

2.2 Production of Single Column Model Initial Analyses.

The UK Meteorological Office possesses an 18 month rolling archive of UKMO Mesoscale Model analysis fields, initial conditions and boundary conditions files at 6 hour intervals (00Z, 06Z, 12Z and 18Z). Therefore for the Cardington fog cases it was a relatively simple matter to retrieve the appropriate mesoscale analyses from the archive. One of these analyses (12Z), once interpolated to the single column resolution (as documented in Clark *et al.*; 1996) provided the initial conditions, whilst the forcing data described below was derived using the Mesoscale model with data assimilation (including surface observations, radiosondes and cloud) up to 12Z to forecast out to T+24 using forecast boundary conditions from the UKMO Limited Area model. Unfortunately the Mesoscale Model archive does not extend far enough back in time to include the Lesquin airport fog cases and hence a different approach had to be used. Fortunately the European Centre for Medium Range Weather Forecasting (ECMWF) MARS archive does extend far enough back to include the Lesquin airport fog cases and ECMWF analyses at 6 hour intervals (06Z to 06Z+24) were retrieved for these cases. These analyses were based upon the ECMWF grid, orography and ancillary fields files. Hence they had to be first re-configured to the UKMO Global model resolution, orography and ancillary files, then further re-configured to the UKMO Mesoscale model resolution and orography. These analyses were then interpolated to provide a 06Z analysis plus 'analysed' boundary conditions. The mesoscale model was then run with these coarse scale analyses to provide the mesoscale detail. At this stage they were ready for interpolation to the single column vertical resolution and to generate the forcing data described below.

3 Current State of the Art: Improvements to the Single Column UM.

The conclusions documented in Clark *et al.* (1996) identified two key areas within which the USCM could be improved for fog forecasting.

The first area was that of parametrization deficiencies. In particular, a more theoretically sound treatment of the surface exchange under stable conditions and a better treatment of the surface moisture and heat transport.

The second area was that of external forcing. The simple, constant geostrophic forcing employed in Clark *et al.* (1996) although a useful tool in forecasting fog formation in relatively stationary mesoscale conditions, produced timescales for dissipation that were much longer than those observed in reality. The answer was to couple the USCM to time varying pressure gradient and advection terms taken from the larger scale Mesoscale model. This would ensure that phenomena such as the passage of fronts and advection of stratocumulus cloud decks would be treated in a way consistent with the large scale flow.

These areas are addressed below:

3.1 Parametrizations.

Clark *et al.* (1996) identified areas where the land surface exchange scheme within the single column UM was not appropriate for local use and hence could not produce an accurate simulation of dew or fog (or both) formation. The treatment of the amount of moisture and heat lost and gained by the land surface was one such area. In the existing scheme the state of the land surface was defined by seven prognostic variables: the available soil moisture content, the canopy water content, the amount of lying snow, the surface temperature and three soil temperature levels. The 'surface temperature' represented the mean temperature of the top soil layer whose thickness depended upon soil type. This formulation has the potential to associate unrealistic thermal inertia with the surface temperature. The hydrology was single layer implying a constant stomatal resistance, constant thermal properties depending upon soil type, no account of phase changes within the soil and no water transport. In order to remedy some of the more important limitations of the above land surface description a new scheme ('MOSES' - Met Office Surface Exchange Scheme) has been designed. This new scheme has the following properties:

- i) 'Surface' Temperature - A Penman-Monteith surface energy balance with a diagnosed 'skin' surface temperature.
- ii) Soil Moisture Vertical Profile - Four soil moisture levels to allow a variation in the soil moisture profile and to provide a near surface moisture variable for use in the bare soil evaporation calculations.
- iii) Soil Hydraulic Properties - 'Effective' soil hydraulic characteristics are derived from the mean fractions of sand, silt and clay within a gridbox using the regression relations of Cosby *et al.* (1984)
- iv) Soil Thermal Properties - Uses coincident soil temperatures and moistures to introduce moisture dependent soil thermal properties.
- v) Soil Water Phase Changes - Inclusion of a parametrization of soil water phase change

based on the 'effective' heat capacity approach of Williams and Smith (1989), where the maximum unfrozen soil water at a given temperature is derived from the soil water suction curve (Black and Tice, 1988).

vi) Surface 'Stomatal' Resistance - The response of stomatal conductance to short wave radiation, temperature, CO_2 concentration and humidity deficit is included in a model of 'Bulk Stomatal' resistance based upon the observed link between photosynthesis and stomatal conductance. This makes use of separate models of C3 and C4 photosynthesis (Collatz *et al.* 1991, 1992) and assumes that the ratio of internal to external CO_2 concentration depends only on the humidity deficit experienced by the plant canopy (Morison and Gifford, 1983). Together these assumptions yield predictions of canopy conductance dependent on temperature, humidity deficit, photosynthetically active radiation, soil moisture content and atmospheric CO_2 concentration.

Clark *et al.* (1996) also specifically outlined the 'surface' temperature parametrization within the surface exchange scheme as inappropriate for local use. The scheme in place for the integrations carried out in Clark *et al.* (1996) neglected any coupling of the surface to the vegetation canopy. The MOSES surface exchange, despite the change in the definition of 'surface' temperature, also neglects the surface to canopy coupling. Therefore as recommended in Clark *et al.* (1996) this treatment has been replaced by a scheme that

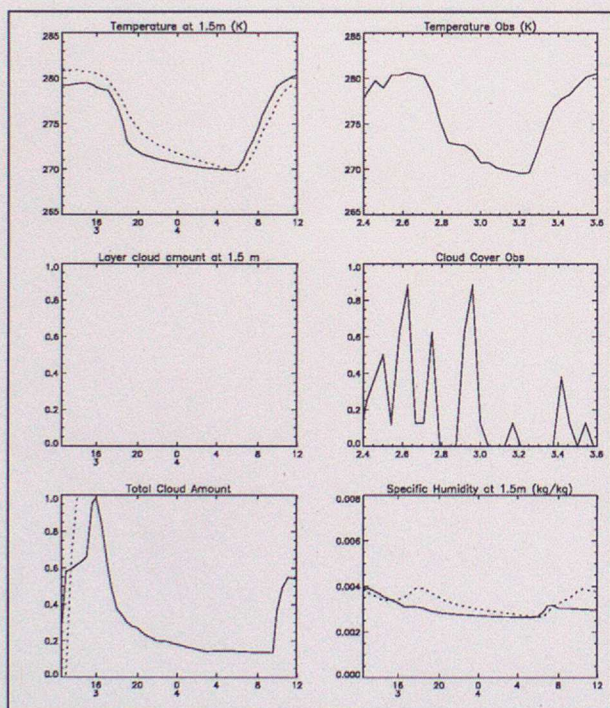


Figure 1a - Intercomparison of 'old' (dotted) and 'new' (full) surface exchange schemes (left). Comparison with relevant observations is also shown.

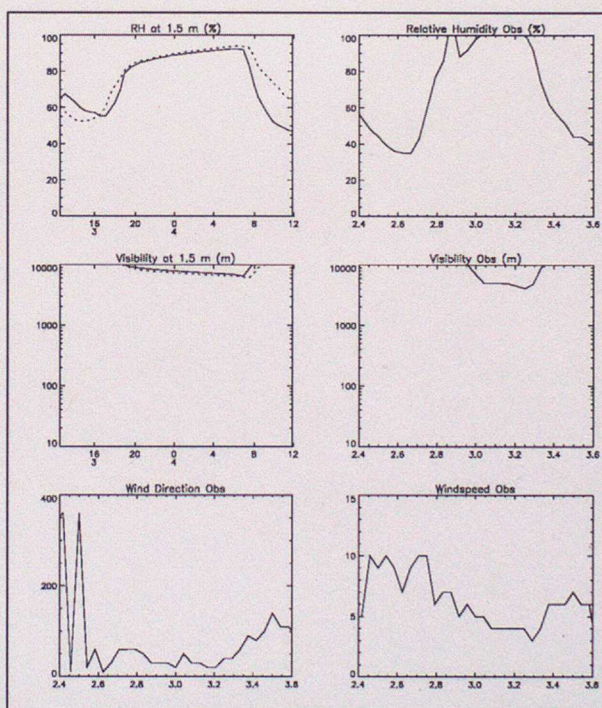


Figure 1b - Intercomparison of 'old' (dotted) and 'new' (full) surface exchanges schemes. Comparison with relevant observations is also shown.

incorporates a vegetation canopy. This scheme, described in detail in Best (1996), removes the ground flux from the energy balance equation that calculates the surface temperature. The canopy then becomes linked to the substrate surface by radiation and turbulent fluxes alone.

The differences between the surface exchange schemes used to compile the interim report and the MOSES scheme with the 'Best' vegetation canopy can be seen for the non-fog Cardington case in Figures 1 (a,b). The forcing used in these integrations is the constant geostrophic forcing outlined in Clarke *et al.* (1996). For the non-fog case (2/3-iv-1996) the two exchange schemes behave similarly reproducing the form of the observed temperature time-series. However, the old scheme produces an overestimate of the daytime maximum which leads to an underestimate in the nighttime temperatures given to same nocturnal cooling rate. This is because the air temperature in the old scheme follows the surface temperature as if the surface were a concrete slab. The introduction of the vegetation canopy scheme corrects for this anomaly.

3.2 Forcing the Single Column UM with output from 3D NWP output systems.

Clark *et al.* (1996) identified that to produce realistic fog dissipation timescales as well as accounting for the passage of fronts and advection of cloud decks the single column model should be coupled to the pressure gradient and advection terms derived from larger scale mesoscale model. The method for doing this is set out below.

3.2.1 Principles

Before discussing the full system, it is easiest to consider a simplified system: a 2D (x-z) dry model with a flat surface. Hydrostatic dynamics will be assumed, and the only subgrid variability in the system to be considered is a variation in surface boundary condition caused by varying surface type.

$$\frac{\partial u}{\partial t} = -u \frac{\partial u}{\partial x} - w \frac{\partial u}{\partial z} + f(v - v_G) - \frac{\partial \overline{u'w'}}{\partial z} - \frac{\partial \overline{u'^2}}{\partial x} \quad (1)$$

$$\frac{\partial v}{\partial t} = -u \frac{\partial v}{\partial x} - w \frac{\partial v}{\partial z} - f(u - u_G) - \frac{\partial \overline{v'w'}}{\partial z} - \frac{\partial \overline{uv'^2}}{\partial x} \quad (2)$$

$$\frac{\partial \theta}{\partial t} = -u \frac{\partial \theta}{\partial x} - w \frac{\partial \theta}{\partial z} + \frac{\theta}{c_p T} Q - \frac{\partial \overline{\theta'w'}}{\partial z} - \frac{\partial \overline{\theta'u'}}{\partial x} \quad (3)$$

Here, the pressure gradient has been described as the equivalent geostrophic wind, (u_G, v_G) in the usual way. Q represents the diabatic heating rate, from radiation and (in a moist model) condensation processes. The full continuity equation is given by:

$$\frac{\partial \rho}{\partial t} + \frac{\partial \rho u}{\partial x} + \frac{\partial \rho w}{\partial z} = 0 \quad (4)$$

though in practice we shall ignore the first term and use this to derive w from the convergence of u . The current discussion is concentrating on flat surfaces and does not intend to consider situations with strong local updraft, so the terms in w will be very small.

The last terms in equations 1 to 3 represent the turbulent fluxes, primarily within the boundary layer. The overbar represents the ensemble mean, and no spatial averaging is implied. It is usual to ignore the last 'along stream' component as it is submerged in the horizontal diffusion required for numerical reasons, but it is included for completeness here.

The large scale model has a grid size with length scale L , and we can define an operator $\langle \rangle_L$ which performs averaging or filtering on this spatial scale. In other words, the u component of wind, for example, in the large scale model is denoted $\langle u \rangle_L$, and we can define the subgrid deviation of any variable f by:

$$f = \langle f \rangle_L + f_s \quad (5)$$

Using this decomposition we can rewrite equations 1-3 as:

$$\frac{\partial u}{\partial t} = -u \frac{\partial \langle u \rangle_L}{\partial x} - u \frac{\partial u_s}{\partial x} - (\langle w \rangle_L + w_s) \frac{\partial u}{\partial z} + f(v - \langle v \rangle_L - v_{G_s}) - \frac{\partial \overline{u'w'}}{\partial z} - \frac{\partial \overline{u'^2}}{\partial x} \quad (6)$$

$$\frac{\partial v}{\partial t} = -u \frac{\partial \langle v \rangle_L}{\partial x} - u \frac{\partial v_s}{\partial x} - (\langle w \rangle_L + w_s) \frac{\partial v}{\partial z} - f(u - \langle u \rangle_L - u_{G_s}) - \frac{\partial \overline{v'w'}}{\partial z} - \frac{\partial \overline{uv'^2}}{\partial x} \quad (7)$$

$$\frac{\partial \theta}{\partial t} = -u \frac{\partial \langle \theta \rangle_L}{\partial x} - u \frac{\partial \theta_s}{\partial x} - (\langle w \rangle_L + w_s) \frac{\partial \theta}{\partial z} + \frac{\theta}{c_p T} Q - \frac{\partial \overline{\theta'w'}}{\partial z} - \frac{\partial \overline{\theta'u'}}{\partial x} \quad (8)$$

It should be noted that the decomposition here is not complete, in that the local values available in the 1D model are used where possible. Thus, the local horizontal velocity is used in the advection term, but the gradient is decomposed into large and small scale. The turbulent and diabatic terms are derived using local parametrizations, as far as possible.

Since we are, primarily, interested in weakly advective situations, we ignore (at this stage) the local component of the vertical velocity (i.e. $w_s=0$). This is a limitation which will be addressed in future versions of the model. It must be recognised that, in strongly stable situations, the main impact of this is that we assume the model surface has the same slope

as the large scale model (generally small). For similar reasons, we also ignore the local component of the horizontal pressure gradient. (The two are clearly related, especially in situations where the hydrostatic approximation applies).

The remaining terms involve either variables directly available in the 1D model, the values of the large scale field or the gradients thereof or the horizontal gradient of the local perturbation. The second of these is derived directly from the output from the large scale model or by numerical differentiation of it, and represents the primary coupling term. The last is the only remaining class of terms requiring parametrization.

The last term represents local advection, i.e. the advection of the perturbation from the large scale. If we consider a region with different surface characteristics embedded in the larger scale mean, then a simple parametrization of this term is given by:

$$u \frac{\partial f_s}{\partial x} = \|u\| \frac{(f - \langle f \rangle_L)}{l_x} \quad (9)$$

where l_x is the upwind fetch. Here, the argument is that at the start of the patch with 'local' characteristics, the variable has a value approximately equal to the large scale mean. This parametrization has been tested in 2D and 1D versions of a detailed boundary layer model (BLASIUS) and has been shown to enable the 1D version to give results quite comparable to the 2D model when simulating flow over a surface inhomogeneity.

This term, of course, represents a Newtonian relaxation onto the large scale flow. As well as representing the effect of local advection, it ensures that the solution derived from the large scale forcing terms does not stray too far from the large scale model. In practice, we expect our higher resolution simulation to differ from the grid box mean for reasons other than the different local surface (e.g. different radiative flux divergence) so we have used different effective fetches at different levels. At very high altitude (i.e. stratosphere) the effective fetch is chosen to be short enough to ensure that the single column is essentially identical to the large scale model. Similarly, in most of the troposphere, a short relaxation timescale of 5 minutes is chosen. In the boundary layer, we have the choice of choosing a relatively long fetch, either representing the real fetch over the surface of interest or the 'gridbox' being simulated, or turning off this term altogether. In the latter case, since we are forcing only with the gradients of the large scale fields, we can derive the maximum impact of both improved model physics and of initial data.

3.2.2 Forcing Equations

The forcing terms are applied to the cloud-conserved variables liquid water potential temperature (θ_l) and total water (q_t) defined by:

$$\theta_L = \theta - (L_c q_c + (L_c + L_f) q_f) / (c_p \Pi) \quad (10)$$

$$q_t = q + q_c + q_f \quad (11)$$

where Π is the Exner pressure given by:

$$\Pi = (p/p_0)^{R/c_p} \quad (12)$$

q_c and q_f are the liquid and frozen cloud, and L_c and L_f are the latent heats of condensation and of freezing.

Since the model actually uses hybrid vertical coordinates (η) the model equations are as follows:

$$\begin{aligned} \frac{\partial u}{\partial t} = & -u \cdot \nabla_{\eta} \langle u \rangle_L - k_r(\|u\|, \eta) (u - \langle u \rangle_L) - \langle \dot{\eta} \rangle_L \frac{\partial u}{\partial \eta} \\ & - f k \times (u - \langle u \rangle_L) + F_u \end{aligned} \quad (13)$$

$$\begin{aligned} \frac{\partial \theta_L}{\partial t} = & -u \cdot \nabla_{\eta} \langle \theta_L \rangle_L - k_r(\|u\|, \eta) (\theta_L - \langle \theta_L \rangle_L) - \langle \dot{\eta} \rangle_L \frac{\partial \theta_L}{\partial \eta} \\ & - \frac{1}{\Pi} [(L_c q_c + (L_c + L_f) q_f) / (c_p T)] (R T \omega / c_p p) + F_{\theta_L} \end{aligned} \quad (14)$$

$$\frac{\partial q_t}{\partial t} = -u \cdot \nabla_{\eta} \langle q_t \rangle_L - k_r(\|u\|, \eta) (q_t - \langle q_t \rangle_L) - \langle \dot{\eta} \rangle_L \frac{\partial q_t}{\partial \eta} + F_{q_t} \quad (15)$$

Here, the F terms represent the diabatic terms calculated by the single column model, while k_r represents the 'local advection' term. It should be noted that horizontal Cartesian coordinates have been used and so various metric terms and minor components of the Coriolis terms have been ignored. The last but one term in eq. (14) is a very small correction to allow for the pressure term in the definition of θ_L (as, strictly, it is T_L rather than θ_L that is conserved when cloud forms). The 'vertical velocity' (in pressure terms) ω , is given by:

$$\omega = \frac{\partial p}{\partial t} + \mathbf{u} \cdot \nabla_{\eta} \mathbf{p} + \eta \frac{\partial p}{\partial \eta} \quad (16)$$

The surface pressure (and, hence) that at model levels) is simply taken from the large scale model. Any local pressure perturbation is ignored. Similarly, the horizontal pressure gradient is derived directly from the large scale model.

A limitation of the mesoscale operational output is that data are only available every hour. Forcing data for intermediate times are derived by simple linear interpolation in time. This has been tested against runs forced with data extracted every timestep, and the errors involved found to be very small. Clearly, in fog situations, the advective terms are already very small, and small errors are negligible.

3.2.3 Visibility

In order to compare with observations, and to make forecasts of practical use in aviation, a parametrization of visibility is required. The same parametrization as used in the mesoscale model has been used. This was described fully in Clark *et al.* (1996) so only is summarized here.

Visibility reduction is assumed to be caused entirely by light scattering from airborne particles whose size is determined by the relative humidity or, when liquid water is present, by sharing the available water out over the number of available particles. The particles are modelled using a total 'dry aerosol' mass mixing ratio m . The volume mean radius is assumed to vary as

$$r_m = r_{m0} \left(\frac{m}{m_0} \right)^p \quad (17)$$

where p is a tunable parameter, set to 1/6. This implies a number density N which varies as m^{1-3p} . The reference mean volume radius is 0.16 μm and total number density 500 cm^{-3} corresponding to $m=m_0$.

When no liquid water is present, the moist radius of particles is assumed to vary with RH according to $r = \alpha r_m$, where:

$$\alpha(RH) = (1 - B/\ln(RH))^{\frac{1}{3}} \quad (18)$$

Where actual liquid water is diagnosed in the model, the same number density as above is used but the radius is calculated by distributing the water equally amongst the drops. If q_c is the liquid water mixing ratio then

$$r = \left(\frac{q_c / \rho_w}{\frac{4}{3} \pi N} \right)^{1/3} \quad (19)$$

where the contribution from the dry particle has been assumed to be negligible.

Using either of these formulations for drop radius, we obtain a simple formula for the scattering coefficient β :

$$\beta(RH) = \int \pi Q(r) r^2 (RH, r_d) n(r_d) dr_d \quad (20)$$

where $Q(r)$ is the normalized scattering cross section. If we assume this is constant across the particle spectrum, we obtain:

$$\beta(RH) = \pi Q \overline{Nr^2} = \pi Q \gamma N r^2 \quad (21)$$

Here, γ is the ratio of the mean square radius to the square of the volume mean radius, and is determined by the shape of the size spectrum. Both Q and γ are essentially empirical constants. Clearly, only their product is of interest. We have found $Q\gamma=1.5$ gives reasonably good results.

Finally, the visibility is derived from the scattering coefficient using:

$$\text{vis} = - \frac{\ln \epsilon}{\beta_{\text{air}} + \beta(RH)} \quad (22)$$

with $\epsilon=0.02$ and β_{air} , which represents the scattering by 'clean' air taken to be that required to produce a visibility of 100 km.

In the single column model, the RH and/or cloud water diagnosed at screen level is used in this formula. The aerosol is derived directly from the mesoscale model. Visibility and RH observations are used to derive an initial analysis of aerosol mixing ratio, which is advected through a forecast and supplemented by a simple treatment of pollution and natural sources.

3.2.4 Impact of Coupled Forcing.

The difference between the constant geostrophic forcing employed in Clark *et al.* (1996) and coupling the USCM to time varying pressure gradient and advection terms taken from the larger scale Mesoscale model are shown in Figures 2 (a,b) and 3 (a,b) for the Cardington non-fog and fog cases (2/3-iv-1996, 11/12-xii-1995). The integrations performed with both methods of forcing used the new MOSES surface exchange scheme and the vegetation canopy

scheme documented in (3.1). Therefore differences observed in the integrations reflect the impact of choosing one form of forcing over the other. However it should be noted that, in radiation fog situations, the magnitude of the external forcing should, almost by definition, be small. The main benefit from coupling to the large scale model therefore comes from either the impact of major changes in conditions (*e.g.* strengthening winds) or from advection of cloud over the fog. It is most likely, therefore, to have an impact on fog clearance later in the forecast period.

In Figure 2, as expected for the non-fog case, both methods of forcing produce an evolution comparable with reality. In terms of 1.5m temperature, constant geostrophic forcing produces a better estimate of the nighttime minimum temperature it being 1.5°K colder than that produced forcing terms taken from the larger scale model. This is due to the presence of a greater amount of low-level cloud in the integration containing the forcing terms from the larger scale model. However, the integration with constant geostrophic forcing cools too quickly in the early part of the evening because it underestimates the magnitude of the daytime maximum temperature. The real advantage in choosing forcing with time varying pressure gradient and advection terms taken from the larger scale model can be seen in the fog case shown in Figure 3. The initial nocturnal cooling is treated well by both methods of forcing as they have identical surface exchange schemes. The fog formation time, as diagnosed from the visibility diagnostic, from the time varying method was about 30 minutes early compared to that diagnosed by the constant geostrophic forcing. It should be noted here that the observations shown in Figure 3 were taken at the ESAWS site described in section (2.1.1), *i.e.* 50m above the forecast site. The fog depth in the 07Z BALTHUM profile (not shown) showed a fog layer about 40m deep which explains the transitory nature of the fog

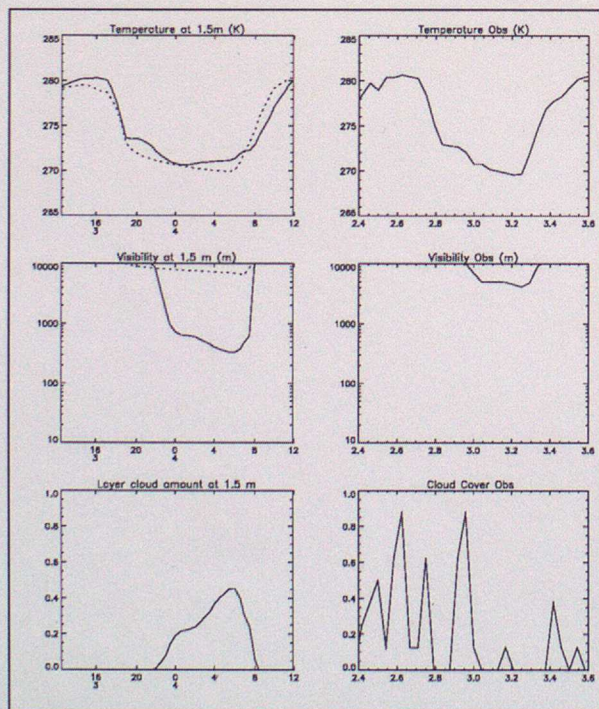


Figure 2a - Intercomparison of constant geostrophic forcing (dotted) and forcing with pressure gradient and advection terms from 3D model (full) for Cardington non-fog case.

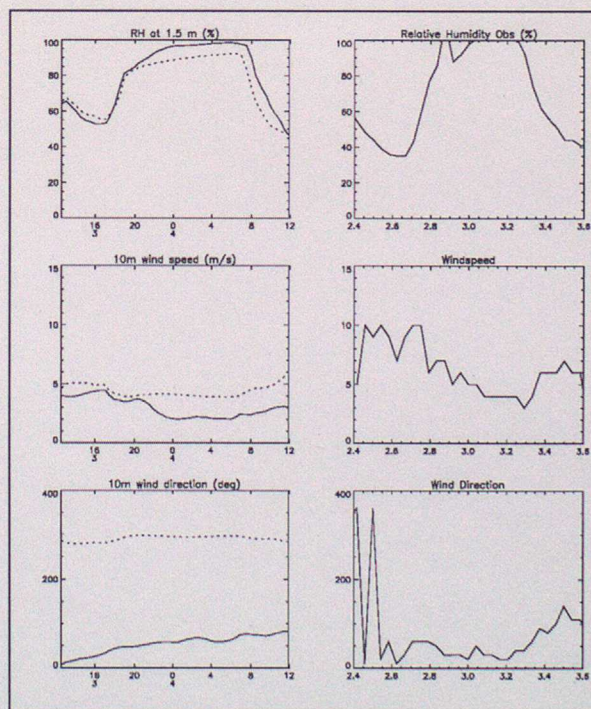


Figure 2b - Intercomparison of constant geostrophic forcing (dotted) and forcing with pressure gradient and advection terms from 3D model (full) for Cardington non-fog case.

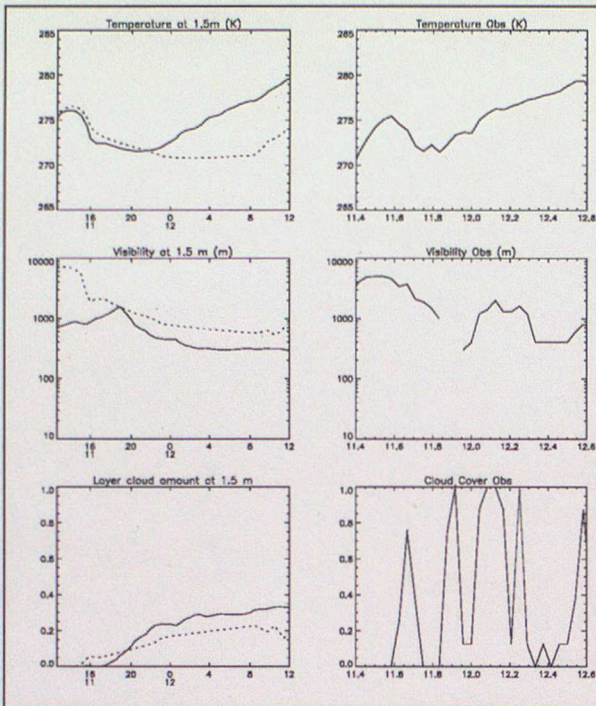


Figure 3a - Intercomparison of constant geostrophic forcing (dotted) with forcing from pressure gradient and advection terms from 3D model (full) for Cardington fog case.

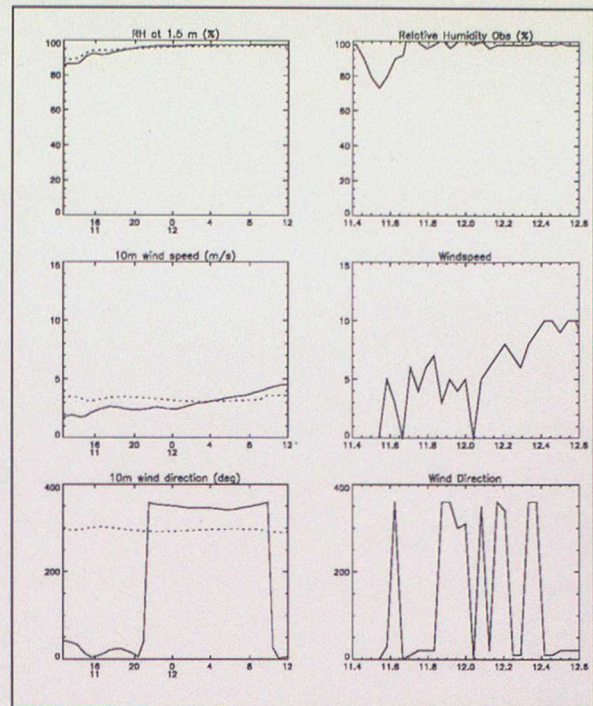


Figure 3b - Intercomparison of constant geostrophic forcing (dotted) with forcing from pressure gradient and advection terms from 3D model (full) for Cardington fog case.

at the ESAWS site.

4 Sensitivity Study of Most Critical Observable Quantities

The impact on the evolution of the high resolution single column model of initialising with observations depends upon two main factors. The accuracy of initial conditions derived from the larger scale 'driving' model and the timescale with which any initial profile relaxes back to the large scale flow. The first factor can be re-written in a more pragmatic fashion as: given that the model initial conditions derived from the larger scale are to some extent in error, which variables have the greatest impact on the model forecast and hence would benefit from being replaced by in-situ observations. To assess the impact of data the model was integrated from initial profiles where the model initial conditions were replaced by wind, temperature and humidity data in various combinations. Only data up to the model level corresponding to the observed boundary layer height at the initialisation time was used. The data used at the Cardington site was derived from 12Z BALTHUM profiles whereas the data used for the Lesquin site was from radiosonde ascents conducted at 15Z. Hence the effect of different initialisation times could also be investigated. These combinations, with identification codes to distinguish them on subsequent figures, were:

- a) Wind data only: CODE - UV,
- b) Temperature data only: CODE - T,
- c) Wind and Temperature data: CODE - UVT,
- d) Wind, Temperature and Humidity data: CODE - UVTQ,
- e) Temperature and Humidity data: CODE - TQ.

The second factor is of course reliant on the type of coupling between the single column model and the pressure gradient and advection terms derived from the larger scale model. The importance of the relaxation timescale to the model evolution is dependent on the initial start time of the forecast. For example, Clark *et al.* (1996) concluded that one of the most important model evolutionary features to correctly predict in order to subsequently predict fog formation was the evening transition cooling rate. The influence of observational data is going to have its greatest impact in determining the 'strength' of the evening transition. So if the model initialisation time is not sufficiently close the time of evening transition then the model profile will have been relaxed back from the observed profile to the large scale flow profile and the influence of the data at initialisation time will have been lost. Therefore in summary, the magnitude of the relaxation timescale combined with the initialisation time of the model determines what impact the inclusion of observational data has on the final forecast. To assess the impact of the relaxation timescale the above combinations of data substitution into the initial profile were implemented on two relaxation formulations. These formulations were:

- a) Relaxation to the large scale flow from the surface to the top of the model, as described in the section (3.2) on forcing - 'total relaxation'.
- b) Relaxation only above the top of the boundary layer - 'partial relaxation'.

4.1 Results of Implementing 'Total Relaxation'.

The results of implementing 'total relaxation' on the Cardington 'non-fog' case (2/3-iv-1996) and the Cardington 'fog' case (12/13-xii-1995) are shown in Figure 4 (a,b & c) and Figure

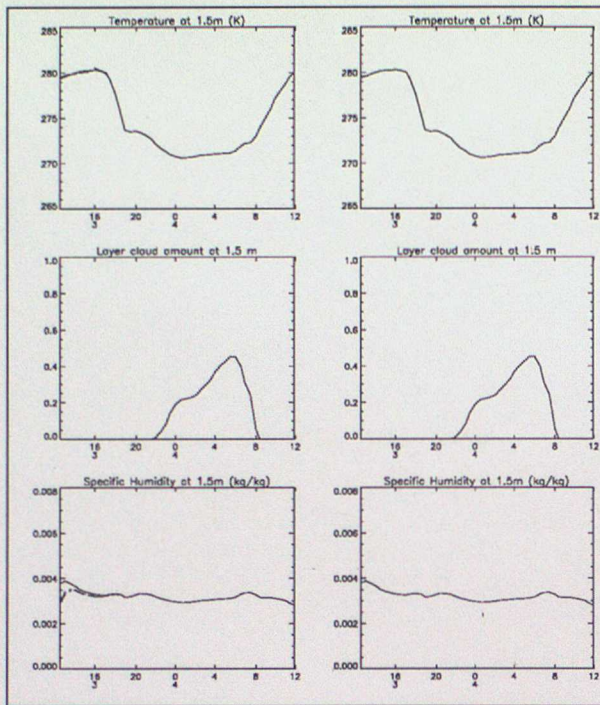


Figure 4a - Evolution curves for various initial data, full relax'n, Cardington non-fog case. No data (full); Left: UV (dotted), UVT (dashed) & UVTQ (dot-dash); Right: T (dotted) & TQ (dashed).

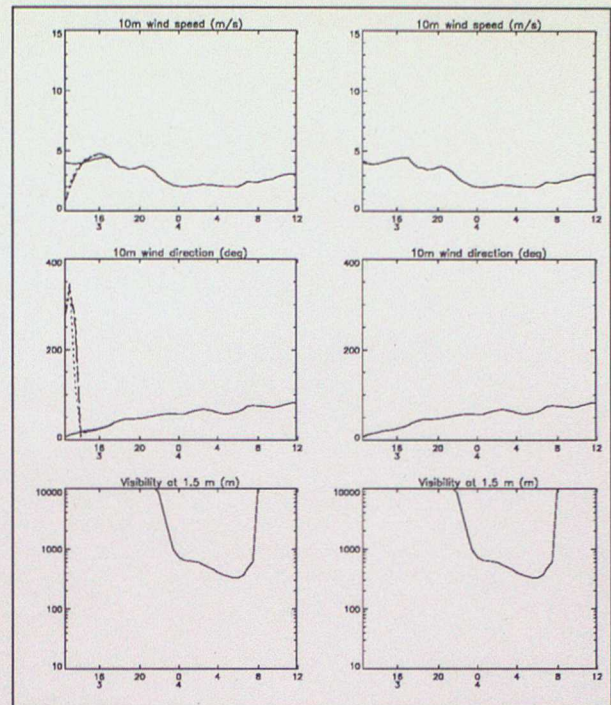


Figure 4b - Evolution curves for various initial data, full relax'n, Cardington non-fog case. No data (full); Left: UV (dotted), UVT (dashed) & UVTQ (dot-dash); Right: T (dotted) & TQ (dashed).

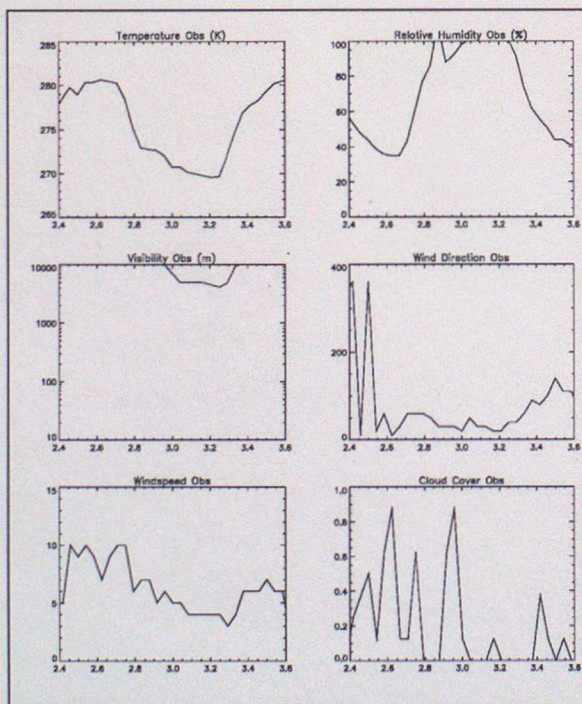


Figure 4c - Timeseries of synoptic observations for the period covering the model integrations.

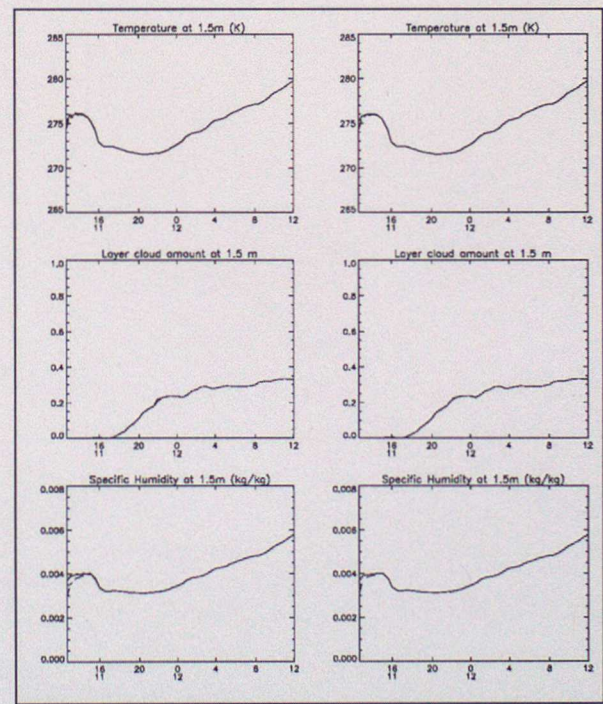


Figure 5a - Evolution curves for various initial data, full relax'n, Cardington fog case. No data (full); Left: UV (dotted), UVT (dashed) & UVTQ (dot-dash); Right: T (dotted) & TQ (dashed).

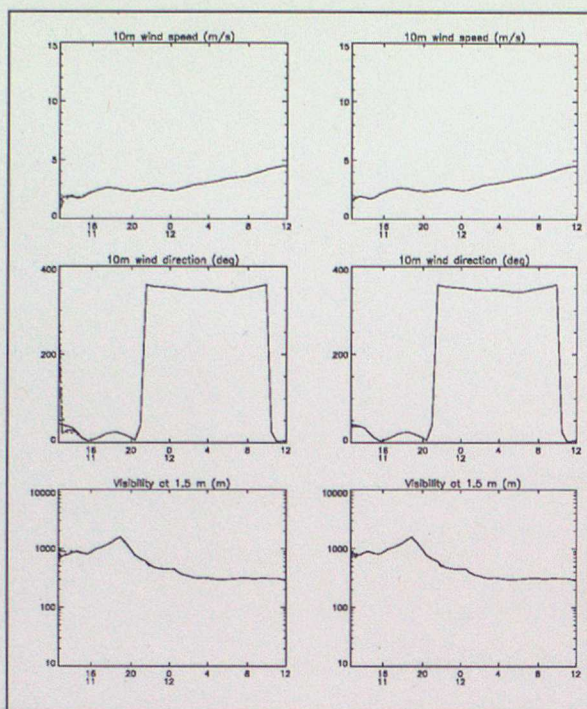


Figure 5b - Evolution curves for various initial data, full relax'n, Cardington fog case. No data (full); Left: UV (dotted), UVT (dashed) & UVTQ (dot-dash); Right: T (dotted & TQ (dashed).

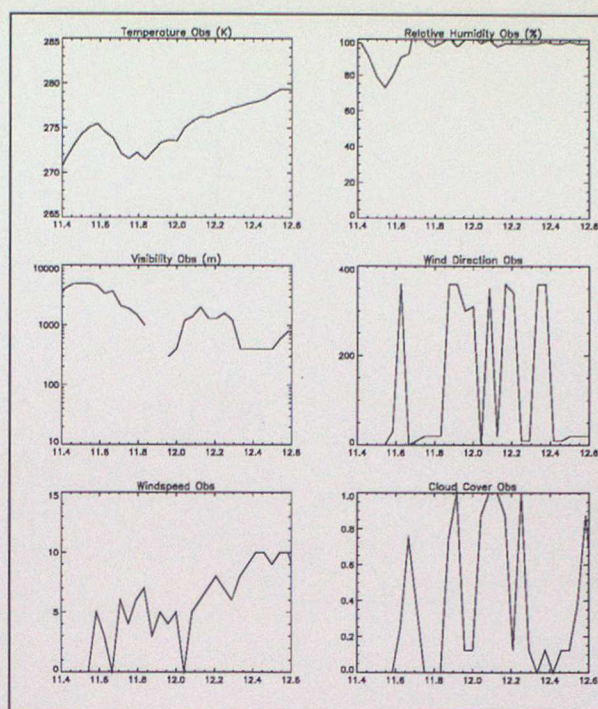


Figure 5c - Timeseries of synoptic observations for the period covering the model integrations.

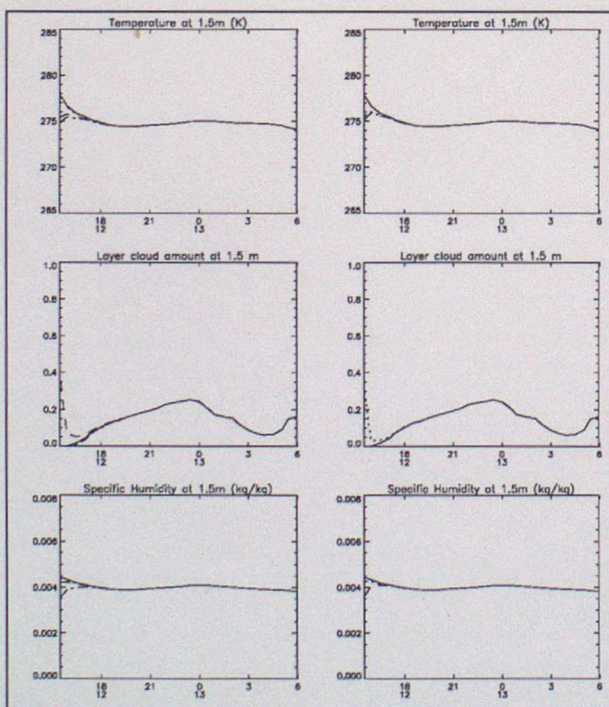


Figure 6a - Evolution curves for various initial data, full relax'n, Lesquin non-fog case. No data (full); Left: UV (dotted), UVT (dashed) & UVTQ (dot-dash); Right: T (dotted) & TQ (dashed).

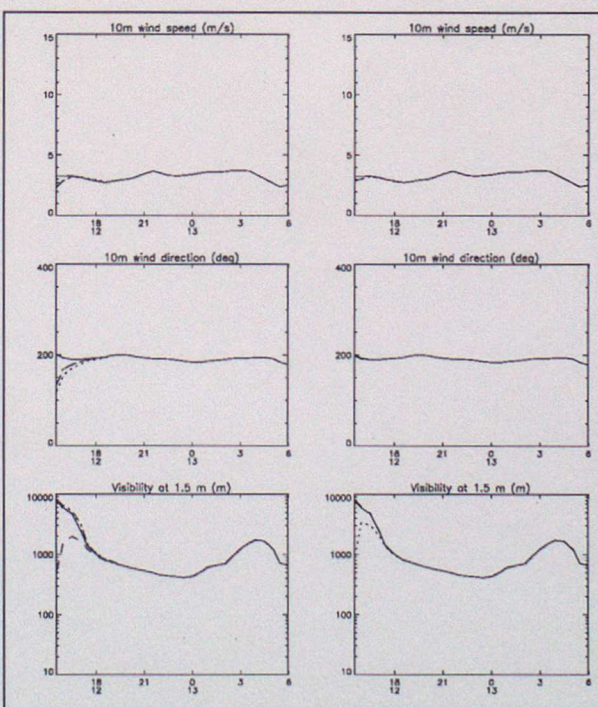


Figure 6b - Evolution curves for various initial data, full relax'n, Lesquin non-fog case. No data (full); Left: UV (dotted), UVT (dashed) & UVTQ (dot-dash); Right: T (dotted) & TQ (dashed).

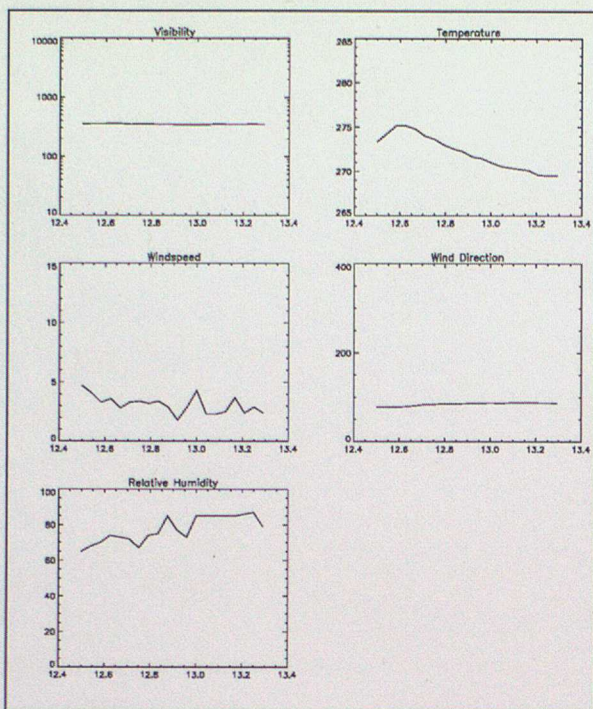


Figure 6c - Timeseries of 5m mast observations for the period covering the model integrations.

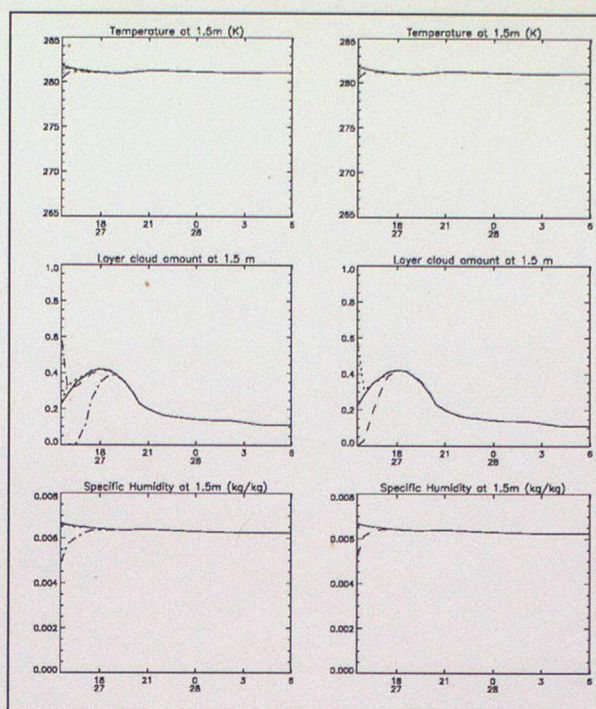


Figure 7a - Evolution curves for various initial data, full relax'n, Lesquin fog case. No data (full); Left: UV (dotted), UVT (dashed) & UVTQ (dot-dash); Right: T (dotted) & TQ (dashed).

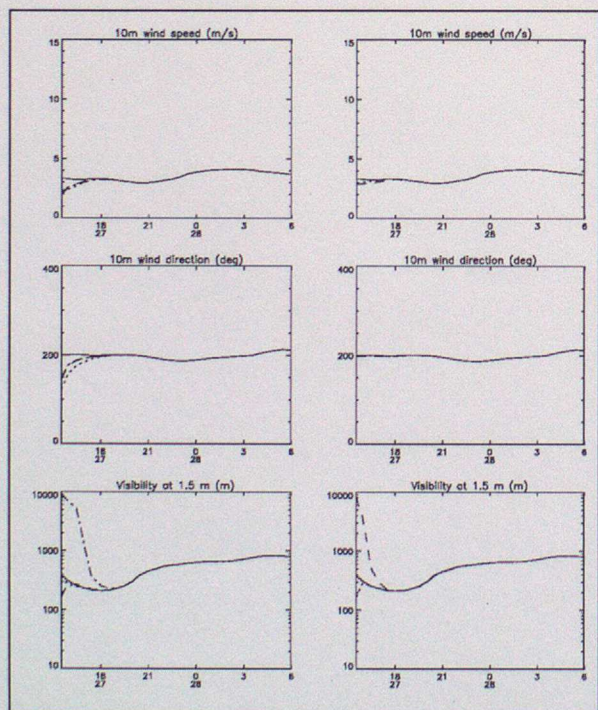


Figure 7b - Evolution curves for various initial data, full relax'n, Lesquin fog case. No data (full); Left: UV (dotted), UVT (dashed) & UVTQ (dot-dash); Right: T (dotted) & TQ (dashed).

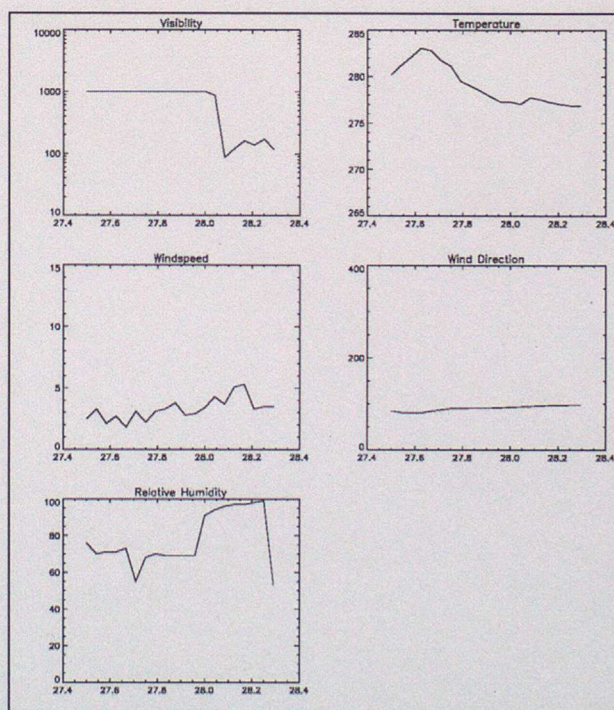


Figure 7c - Timeseries of 5m mast observations for ht period covering the model integrations.

5 (a,b & c) respectively. These integrations were initialised at 12Z.

Both these figures show that the relaxation back to the large scale is within 3 hours of the initialisation time. Given that the initialisation time was 12Z, the evolution of the integrations with observational data substituted into their initial profiles through evening transition and beyond, was identical to those integrations performed with an initial profile taken directly from the larger scale model. *i.e.* no combination of data had any impact upon the final forecast. This can be understood by considering the Mesoscale grid box. Air within a gridbox is completely replaced within 3 hours for a windspeed as low as 1.6ms^{-1} . Thus, it is impossible to maintain consistency between forecasts unless the local impact of observations is short lived. The results of implementing 'total relaxation' on the Lesquin 'non-fog' case (12/13-xii-1991) and the Lesquin 'fog' case (27/28-xi-1991) are shown in Figure 6 (a,b & c) and Figure 7 (a,b & c) respectively. These integrations were initialised at 15Z.

As with the Cardington cases relaxation back to the large scale occurs within 3 hours of the initialisation time and although the initialisation was at 15Z the impact on the evening transition was negligible. Hence the influence of the data imported into the initial profile was non-existent. It should be noted that the model evolution in comparison with the observational data at the site is poor. It is particularly noticeable in the cooling curves both in absolute terms and in the rate of cooling. The model is warmer and has a small cooling rate. The reason for this is that the model contains a cloud fraction close to 1 compared to the observations of cloud fractions of approximately 0.1 in both cases. This error has been associated to the method of creating the forcing data and initial analysis, as outlined in sections (2.2) and (3.2), which has little information on the local moisture field. Anticipating later results, importing moisture observations with forcing including 'partial relaxation' corrects the moisture field and hence the cloud fraction producing a 'better' forecast.

4.2 Results of Implementing 'Partial Relaxation'

In practice, errors at one location are correlated with those elsewhere. If new observations were available they would be expected to have an impact on the mesoscale forcing data. Some idea of the maximum benefit to be gained from 'local' observations can be obtained by correcting the forcing data in line with the initial analysis. This is approximately equivalent to turning off the relaxation term. The results of implementing 'partial relaxation' on the Cardington 'non-fog' case (2/3-iv-1996) and the Cardington 'fog' case (12/13-xii-1995) are shown in Figure 8 (a,b,c & d) and Figure 9 (a,b,c & d) respectively. These integrations were initialised at 12Z. Both these figures show that the effect only implementing relaxation back to the large scale flow above the boundary layer increases the timescale over which the data imported into the initial conditions influences the model evolution. This relaxation timescale has been increased from ~ 3 hours to ~ 12 hours. Considering the 'non-fog' case in Figure 8 first; the only impact on the model evolution is seen when humidity data is introduced into the initial profile. Comparison with the model evolution with no included observational data it produces a relative warming of $\sim 0.5\text{K}$ during the night and a relative cooling of $\sim 1.5\text{K}$ during the morning. However when compared to the observations the impact on other

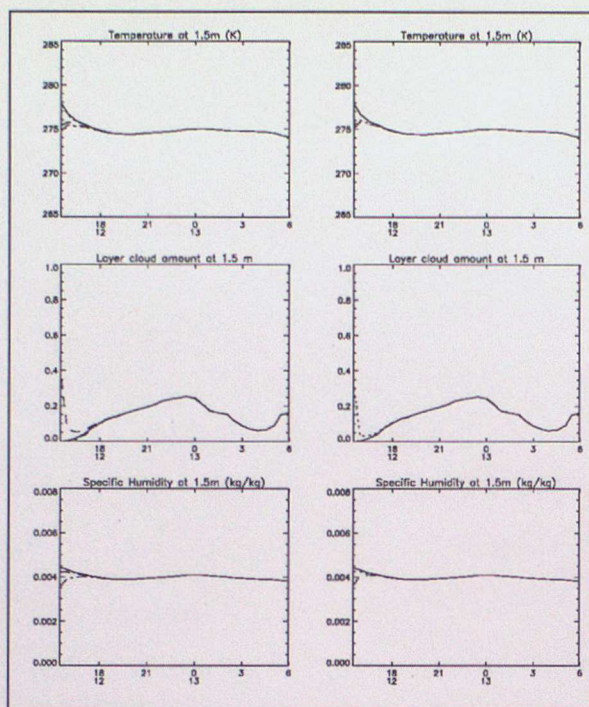


Figure 8a - Evolution curves for initial data, partial relax'n, Cardington non-fog case. No data (full); Left: UV (dotted), UVT (dashed) & UVTQ (dot-dash); Right: T (dotted) & TQ (dashed).

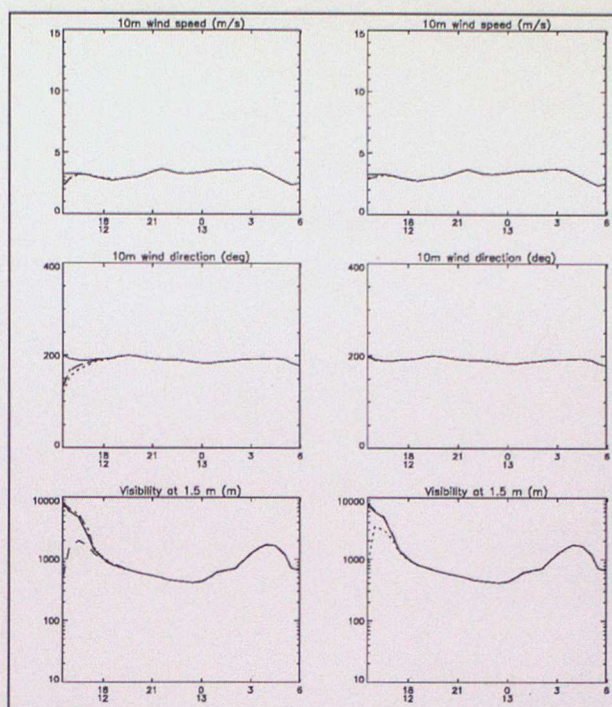


Figure 8b - Evolution curves for various initial data, partial relax'n, Cardington non-fog case. No data (full); Left: UV (dotted), UVT (dashed) & UVTQ (dot-dash); Right: T (dotted) & TQ (dashed)

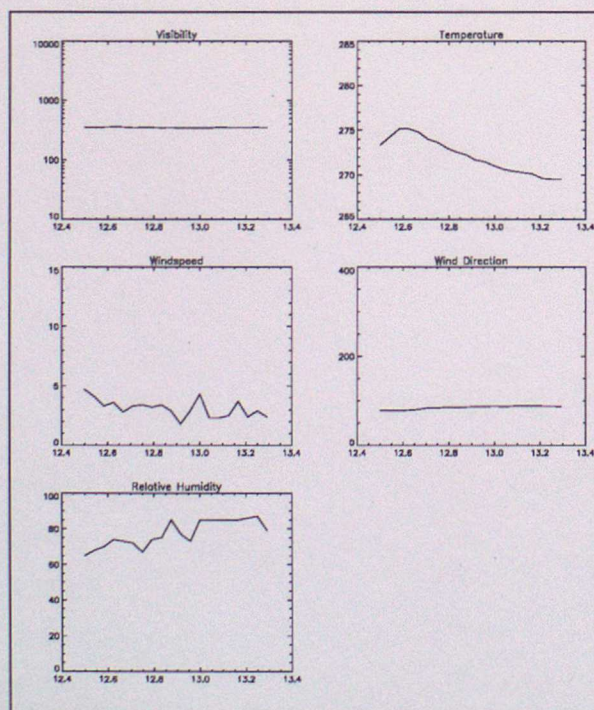


Figure 8c - Timeseries of synoptic observations for the period covering the model integrations.

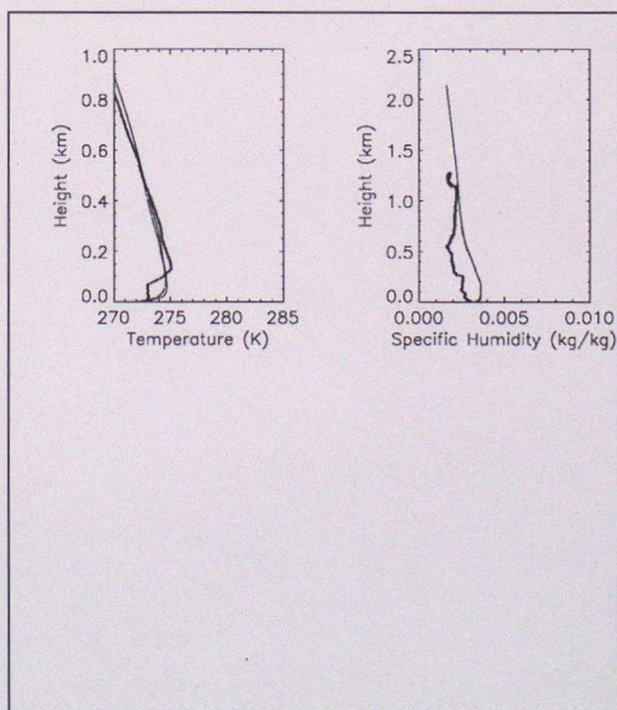


Figure 8d - Intercomparison of model (full) and BALTHUM profiles for 07Z. Left: Temperature; Right: Specific Humidity.

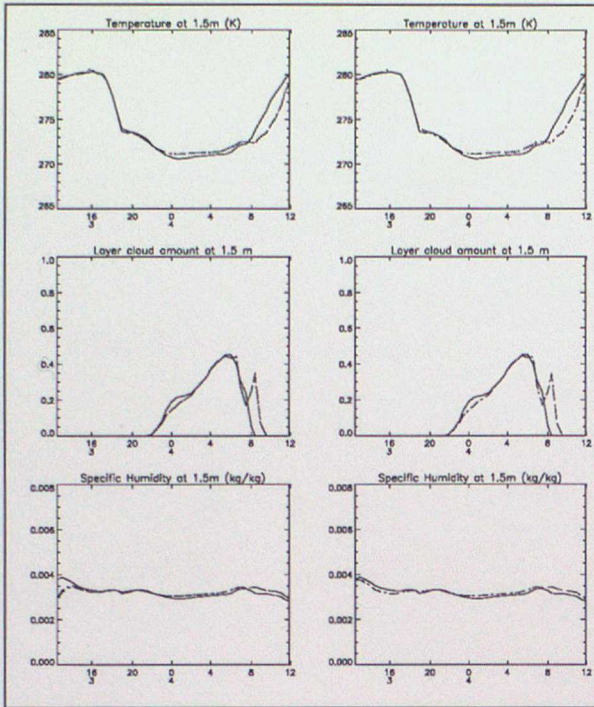


Figure 9a - Evolution curves for various initial data, partial relax'n, Cardington fog case. No data (full); Left: UV (dotted), UVT (dashed) & UVTQ (dot-dash); Right: T (dotted) & TQ (dashed).

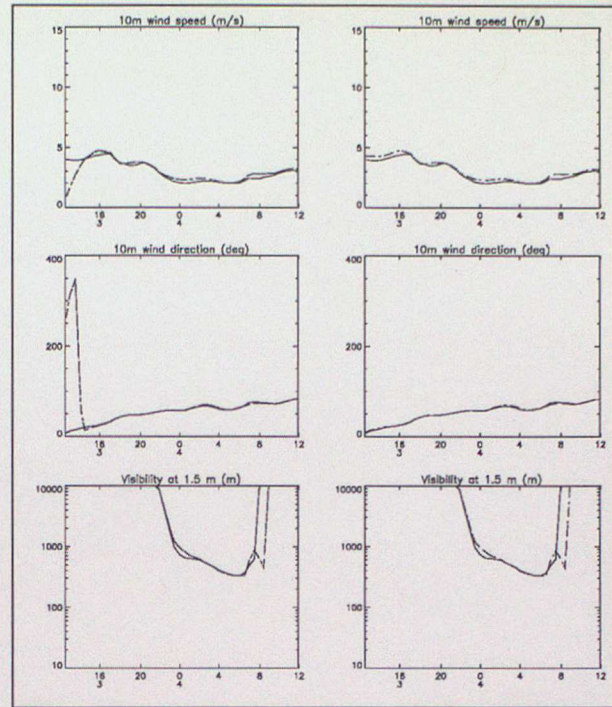


Figure 9b - Evolution curves for various initial data, partial relax'n, Cardington fog case. No data (full); Left: UV (dotted), UVT (dashed) & UVTQ (dot-dash); Right: T (dotted) & TQ (dashed)

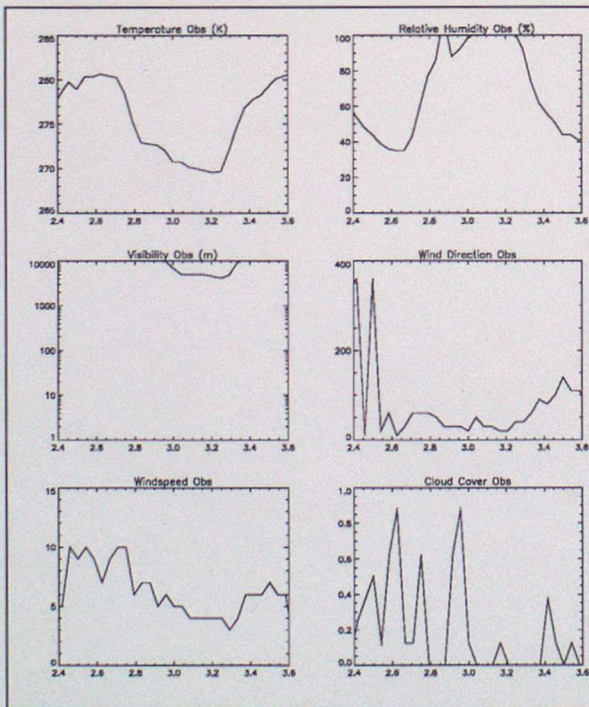


Figure 9c - Timeseries of synoptic observations for period covering the model integrations.

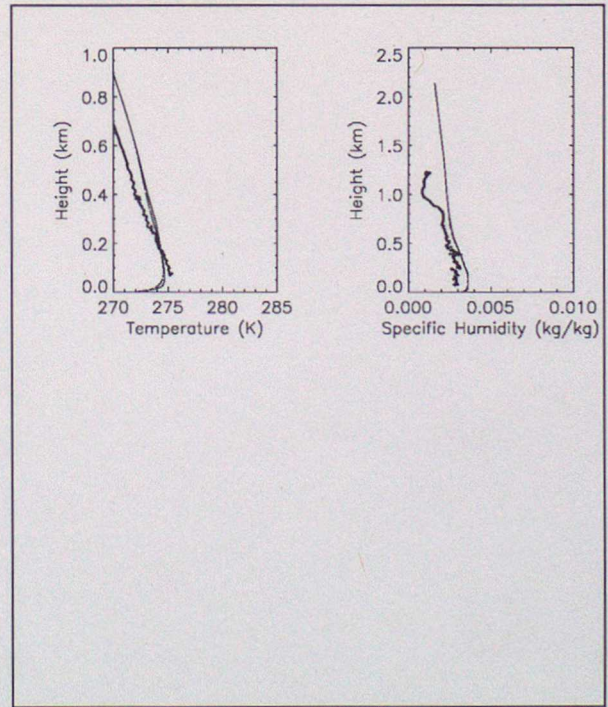


Figure 9d - Intercomparison of Model (full) and BALTHUM profiles for 07Z. Left: Temperature; Right: Specific Humidity.

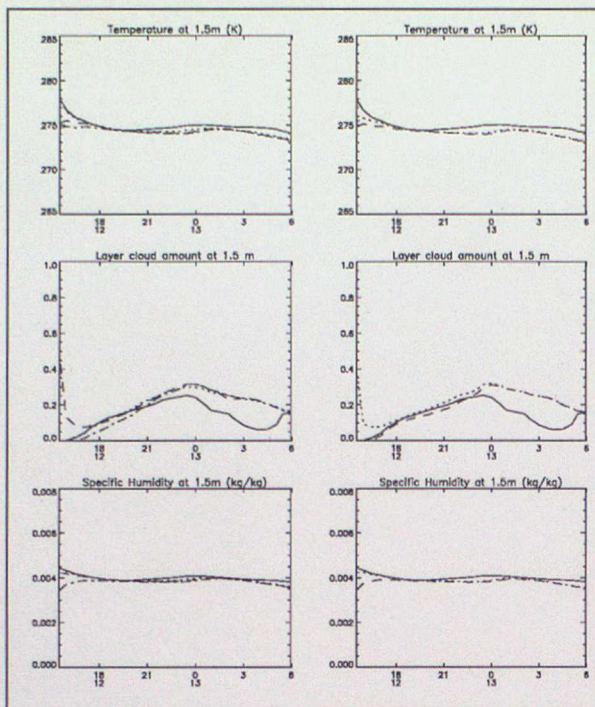


Figure 10a - Evolution curves for various initial data, partial relax'n, Lesquin non-fog case. No data (full); Left: UV (dotted), UVT (dashed) & UVTQ (dot-dash); Right: T (dotted) & TQ (dashed)

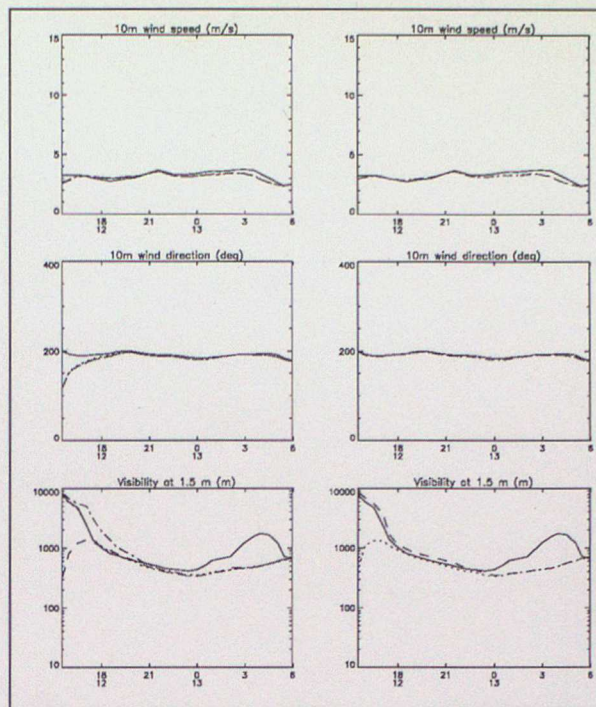


Figure 10b - Evolution curves for various initial data, partial relax'n, Lesquin non-fog case. No data (full); Left: UV (dotted), UVT (dashed) & UVTQ (dot-dash); Right: T (dotted) & TQ (dashed)

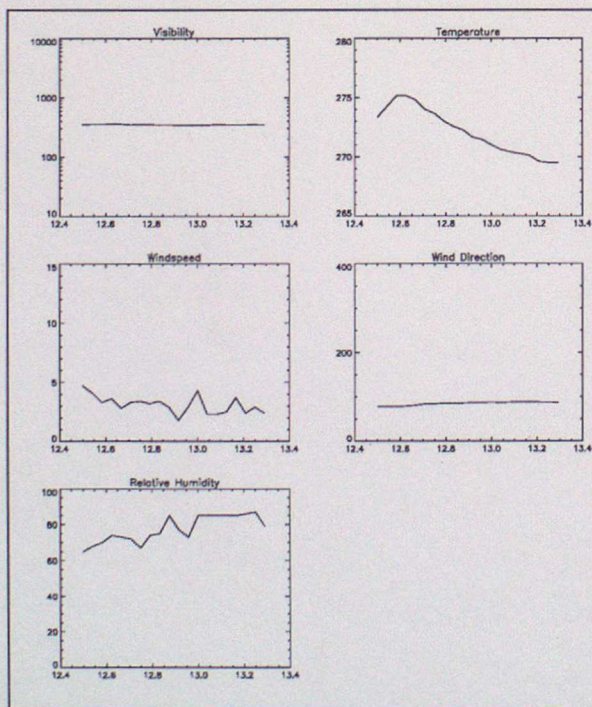


Figure 10c - Timeseries of 5m mast observations for the period covering the model integrations.

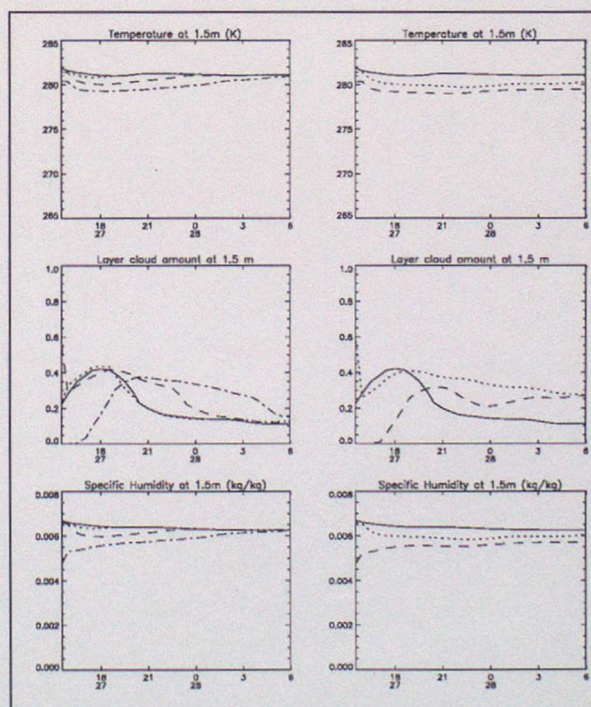


Figure 11a - Evolution curve for various initial data, partial relax'n, Lesquin fog case. No data (full); Left: UV (dotted), UVT (dashed) & UVTQ (dot-dash); Right: T (dotted) & TQ (dashed).

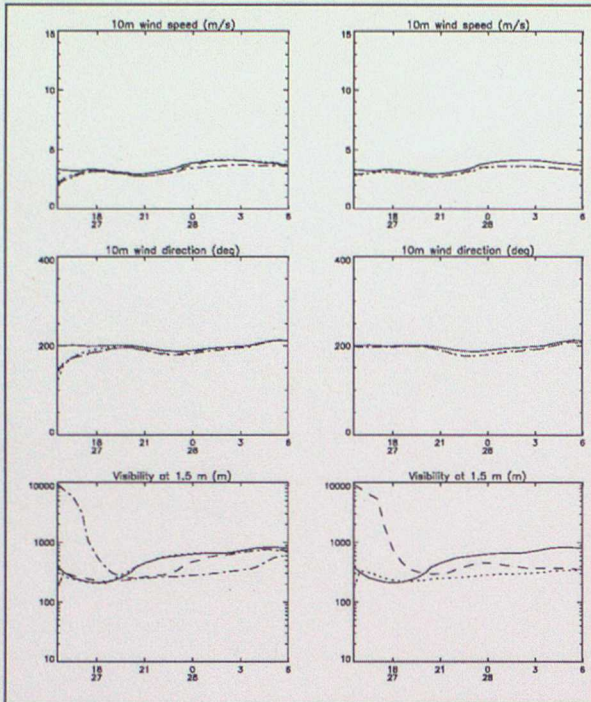


Figure 11b - Evolution curves for various initial data, partial relax'n, Lesquin fog case. No data (full); Left: UV (dotted), UVT (dashed) & UVTQ (dot-dash); Right: T (dotted) & TQ (dashed).

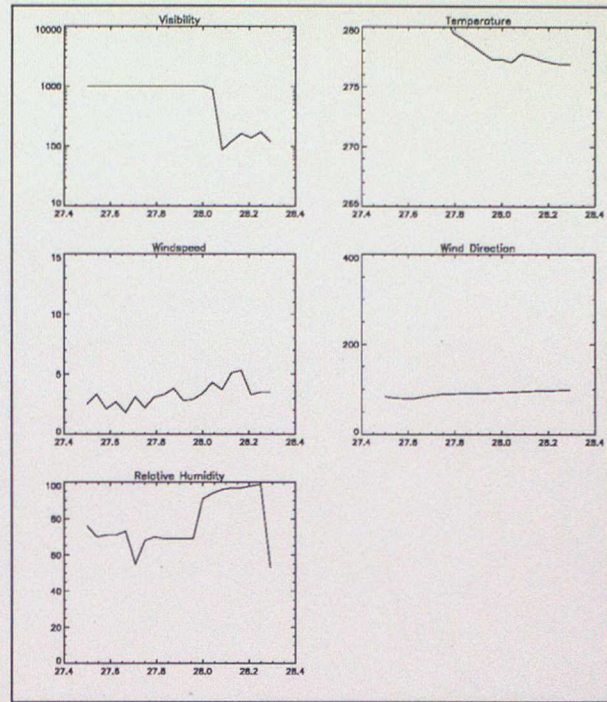


Figure 11c - Timeseries of 5m mast observations for the period covering the model integrations.

parameters is negligible. Moving onto the fog case shown in Figure 9, the temperature evolution does not show a large variation for each combination of observational data imported into the model initial profile. The one significant alteration in the model surface layer temperature evolution occurs when only the temperature data is imported into the initial profile. This produces a warmer near-surface layer during evening transition by about 1K. This warming is eradicated by relaxation back to the large scale profile around midnight. In other variables such as the visibility and 1.5m layer cloud amount diagnostics, both indicators of fog formation, some impact is seen with the inclusion of temperature data with a delay of about 1 hour in the fog formation time. Yet a much larger impact is seen once the humidity data is imported into the initial profile. This evolution clearly delays the onset of fog formation by about 6 hours. The cause of this result can be seen in the specific humidity time series shown in Figure 9a, where the initial moisture profile is observed as being 25% drier than that implied by the larger scale model. This is consistent with the Clark *et al.* (1996) where the sensitivity of fog formation time to initial moisture content showed identical behaviour. The synoptic observations shown in Figure 9c also show similar behaviour.

The results of implementing 'partial relaxation' on the Lesquin 'non-fog' case (12/13-xii-1991) and the Lesquin 'fog' case (27/28-xi-1991) are shown in Figure 10(a,b & c) and Figure 11 (a,b & c) respectively. These integrations were initialised at 15Z.

It can be seen that, as with the Cardington cases, the impact of using a 'partial relaxation' is to increase the time the initial profile influences the model evolution before relaxing back to the large scale flow from ~3 hours to ~12 hours. Considering the 'non-fog' case shown in Figure 10 first, the main impact on the model evolution is generated by including temperature observations into the initial profile. Incorporating the wind and/or humidity data has little

influence on the final outcome of the integration. Moving onto the fog case, shown in Figure 11, then as with the Cardington fog case the greatest impact on model evolution in terms of fog formation occurs when humidity data are incorporated into the initial profile. The fog formation time is delayed by ~4 hours. The cause is again the large scale model which produces a boundary layer that is too moist. The observational data corrects for this by reducing the boundary layer moisture profile by about 30% which translates into a 3-5 hour delay in the fog formation time. It should be noted that the time of fog formation within the model, even with the humidity observations, was 7 hours earlier than reality. In addition the evolution of the surface layer temperature does not mirror reality shown in Figure 11c. The reason for these anomalies is that the large scale model profile is too moist and hence has too much cloud within the boundary layer. This prevents surface radiative cooling and the formation of fog in the normal radiative manner. The fog generated in the model is caused by the boundary layer cloud thickening and descending to the surface. In summary the integrations in this case are not a good simulation of reality.

5 Discussion and Conclusions.

This report has described :

- i) the improvements made to the single column version of the UKMO unified model outlined in Clark *et al.* (1996);
- ii) a sensitivity study to assess which observable quantities are most critical to the initial conditions of a model to produce an improved forecast at a specified time.

The model improvements were two-fold: The surface exchange scheme was replaced with a more sophisticated scheme within which canopy processes were taken into account in the deduction of surface temperature. The result of this is an improved forecast of nighttime cooling rate and temperature forecast, important to fog prediction. The second improvement was the replacement of the constant geostrophic forcing used in stage 1 of the SSFM project (Clark *et al.*, 1996) with a coupled forcing which used time varying pressure gradient and advection terms derived from the Mesoscale model. The motivation for this change, given that under conditions favourable to fog formation the external forcing should by definition be small, was to be able to simulate major changes in conditions during the forecast period and therefore improve the prediction of fog clearance.

The sensitivity study yielded a number of conclusions that are dependent on scale. The local scale and the 'forcing' scale. As a starting point, it can be said that model evolution in synoptic conditions suitable for fog formation is most significantly influenced during the evening transition period (*i.e.* sunset to 00Z). As the impact timescale of any kind of data substituted into the initial conditions of a model is dependent on the strength of the relaxation used by the forcing to push the initial profile back towards the large scale flow, which is typically less than 3 hours. Then the time of model initialisation relative to the time of evening transition becomes important. To this end the French COBEL (Guedalia and Bergot, 1994) model initialisation time of 15Z has an advantage over the USCM 12Z initialisation since the relaxation timescale on the USCM forcing scheme is about 3 hours. This can be seen in the results shown in section (4.1) where the impact of local data was negligible. Having said this, one consideration, important in conditions of potential fog formation, has been neglected. It should be expected that local observations should influence not only the initial profile but also the mesoscale forcing data. The likely benefit of this was assessed in section (4.2) by equating this neglected impact to a restriction in the relaxation to above the observed boundary layer. The greatest impact on forecast evolution was provided by the inclusion of humidity, and to a lesser extent temperature, data where the inclusion of a moisture profile observations that were 15% drier than the model profile delayed the fog formation time by ~6 hours. This integration was within 30 minutes of the observed fog formation time. The influence of wind data was negligible because the large scale mesoscale model does a good job of simulating the wind field. Therefore it is desirable to have local, near-surface humidity data incorporated into the model initial conditions such that they are allowed to influence the model boundary layer during evening transition.

This study has been confined to assessing the impact of importing observational data into the model levels that are within the observed boundary layer at the time of initialisation. In doing so the attempt has been to better describe the controlling mechanisms and all but one of the influencing factors that are important in forecasting fog formation *i.e.* those that to a large

extent occur within the boundary layer. The one factor that has been left out is that of diagnosed cloud cover. This controls the radiative balance at the surface and for the most part (*e.g.* Stratocumulus) is above the boundary layer. The effect it can have can be seen in the Lesquin fog case where Stratocumulus is diagnosed in both the initial profile and the advection part of the forcing. This was not observed synoptically and manifests itself as an overestimate in the model moisture profile. The subsequent forecast shows fog formation but far too early in the forecast and mainly due to a cool daytime temperature profile compared to what was observed. In cases such as these temperature and moisture data from above the boundary layer would be invaluable in correcting model initial profiles and forcing data. The resolution of such data can be relatively coarse above the boundary layer, the necessity within the boundary layer being to capture the boundary layer top inversion with a vertical resolution as close as is possible to that of the model.

To summarise the most important points:

1. The most important observations are those of humidity because,
 - a) the model is sensitive to changes in humidity,
 - b) the large scale model does quite well with wind and to some extent temperature.
2. The local impact of observations lasts only a few (typically less than 3) hours since even in light wind cases advection brings in the large scale air after 6 hours.
3. Therefore forecasts that are initialised late in the afternoon (*e.g.* 15Z rather than 12Z) are much more successful at predicting the onset of fog than from earlier in the day.
4. Observations must also improve the larger scale forecast if benefit is to be gained beyond about 3 hours.

6 References

- Best, M.J. 1996 A model to predict surface temperatures. *submitted to Bound. Layer Met.*
- Black, P.B. & Tice, R.A. 1988 Comparison of soil freezing curve and soil water curve data for Windsor sandy loam. *US Army Cold Regions Research and Engineering Laboratory Report 88-16*, Hanover, NH, US.
- Clark, P.A., Hopwood, W.P., Best, M.J., Dunlop, C.C. & Maisey, P.E. 1996 Assessment of the Single Column UM as a local forecasting tool: suitability and recommended configuration. *Forecasting Research Division Technical Report No. 203*, Meteorological Office, London Road, Bracknell. U.K.
- Collatz, G.J., Ball, J.T., Grivet, C. & Berry, J.A. 1991 Physiological and environmental regulation of stomatal conductance, photosynthesis and transpiration: A model that includes a laminar boundary layer. *Agric. & Forest Met.* **54** 107-136
- Collatz, G.J., Ribas-Carbo, M. & Berry, J.A. 1992 Coupled photosynthesis-stomatal conductance model for leaves of C4 plants. *Aust. J. Plant Physiol.* **19** 519-538
- Cosby, B.J., Hornberger, G.M., Clapp, R.B. and Ginn, T.R. 1984 A statistical exploration of the relationships of soil moisture characteristics to the physical properties of soils. *Water Resources Res.* **20** 682-690
- Guedalia, D. & Bergot, T. 1994 Numerical forecasting of radiation fog. Part II: comparison of model simulation with several fog events., *Mon. Wea. Rev.*, **122**, 1231-1246
- Lapworth, A.J. & Mason, P.J. 1988 The new Cardington turbulence probe system. *J. Atmos. Oceanic Technol.*, **5** 699-714
- Williams, M.F. & Smith, M.W. 1989 'The Frozen earth', Cambridge University Press, Cambridge.